a-axis-projected electron-positron-momentum density and positron-annihilation spectra in $YBa_2Cu_3O_{7-x}$

R. Pankaluoto* and A. Bansil
Physics Department, Northeastern University, Boston, Massachusetts 02115

L. C. Smedskjaer
Argonne National Laboratory, Argonne, Illinois 60439

P. E. Mijnarends
Interfaculty Reactor Institute, Delft University of Technology, Mekelweg 15, 2629 JB Delft, The Netherlands
(Received 28 February 1994)

We present and discuss theoretical and experimental a-axis-projected two-dimensional angular correlation of annihilation radiation (2D-ACAR) spectra from $YBa_2Cu_3O_{7-x}$. The experiment involved an *untwinned* metallic single crystal of $YBa_2Cu_3O_{6.9}$ at room temperature. The calculations have been carried out within the conventional first-principles band-theory framework based on the local-density approximation; the positron state is treated in the independent-particle model. After the as-observed 2D-ACAR spectrum is corrected for an isotropic background, a good accord is found between not only the overall shape but also the fine structure in the measured and computed spectra, some discrepancies notwithstanding. Extensive analysis shows that the experimental spectrum clearly contains the signature of the electron ridge Fermi surface (FS) arising from Cu-O chains in the first Brillouin zone. Also the first and second Umklapp images of the ridge FS at higher momenta are in substantial accord with theoretical predictions. These results suggest that the electron states in Y123 are not localized, at least not strongly, along the c direction.

I. INTRODUCTION

Two-dimensional angular correlation of annihilation radiation (2D-ACAR) positron spectroscopy is a powerful probe of electronic structure in problems where momentum resolution is essential. Efforts to explore the Fermi surfaces (FS's) via this technique in $YBa_2Cu_3O_{7-x}$ (Y123) were started immediately after the discovery of the new superconductors.[1-4] 2D-ACAR measurements together with corresponding first-principles computations within the conventional band theory framework have established unequivocally that Y123 possesses a Cu-O chain related FS sheet parallel to the crystal a direction—the electron ridge, in substantial accord with theoretical predictions based on the local-density approximation (LDA), electron-electron correlation effects notwithstanding. In this connection, good consistency in the experimental[5-14] as well as theoretical[15-19] results using a variety of different methodologies from various independent groups gives great confidence in the 2D-ACAR data and its interpretation. It has also become clear that, since the positron tends to occupy open volumes as it tries to avoid positively charged ionic cores, the positron spatial distribution in a complex crystal will in general be quite nonuniform. In the specific case of Y123, the electron-positron matrix element turns out to be weighted in favor of electron states associated with Cu-O chains.[15,17,20] For these reasons, it is most sensible to view positron annihilation to be complimentary to other **k**-resolved spectroscopies—angle-resolved photoemission (ARPES), de Haas–van Alphen (dHvA), and the emerging technique of high-resolution Compton scattering.[21] Each of these possesses its own strengths and limitations.[1-4] Indeed, the full picture of the FS of Y123 has been pieced together via the combined use of several spectroscopies: the electron ridges through 2D-ACAR as noted, the CuO_2 plane related "barrels" through ARPES,[22,23] and a small "pillbox" hole sheet through dHvA.[24,25] All of these sheets are in essential accord with band-theory predictions. Although Y123 is the most extensively investigated compound, the application of 2D ACAR to a number of other high-T_c materials should be noted.[26-30]

Much of the existing 2D-ACAR work on Y123 has concentrated on the c-axis projection where the measured 2D spectrum is related to the integral of the 3D electron-positron momentum density along the crystal c axis. This focus is natural, since in a layered material the bands will possess a relatively small dispersion along the c direction, and therefore the FS sheets will tend to be in the shape of cylinders extended along the c axis, making the c projection particularly suitable for exploring FS's.[7] In this article, we extend the 2D-ACAR study of Y123, theoretical as well as experimental, to include the a-axis projection. The motivation is severalfold. Most important, some current views hold that there is a fundamental difference in the nature of electron states in various directions in high-T_c crystals, and that the states may in particular become localized perpendicular to the CuO_2 planes.[31,1-4] The c projection is not suited to address this

question because the c-axis integral implicit in the measurement will render the spectrum insensitive to features of the underlying 3D momentum density along the integration direction. The a projection is of interest, of course, also in its own right because it offers another view of the 3D momentum density of Y123, and a further test of the validity of the band-theory model, which has been successful in describing the c projected data. We are not aware of a previous systematic study of the a projection, although some 2D-ACAR data has been reported in Ref. 19.

An outline of this article is as follows. The introductory remarks are followed in Sec. II with a delineation of relevant technical details on the theoretical as well as the experimental side. Section III describes the new experimental and theoretical results and analyzes the structure in the 2D-ACAR spectra in the light of the predicted FS signatures in the a projection; a preliminary report of this work has been presented elsewhere.[14,32] A few concluding remarks, including the implications of this study with regard to possible localization of states along the c direction are made in Sec. IV.

II. EXPERIMENTAL AND THEORETICAL CONSIDERATIONS

The 2D-ACAR measurements were taken at room temperature (300 K) from a nearly *untwinned* $0.9\times1.6\times0.1$-mm^3 single crystal of $YBa_2Cu_3O_{6.9}$; an optical examination of the sample showed the presence of only a few twinned regions of small size. The transition temperature ($T_c=91$ K, $\Delta T=1$ K) was measured before and after the completion of the experiment to ensure that no degradation of the sample took place during the measurements. In order to obtain the a-axis projected spectrum, the crystal a-axis was aligned carefully along the camera axis by reflecting a laser beam from the sample surface. The alignment of the b and c axis of the specimen is less critical, since the exact orientation in this case can be determined by analyzing the symmetry of the spectra.[33]

The momentum resolution [full width at half maximum (FWHM)] due to the camera and sample size was 0.4–0.5 mrad; when the effect of positron thermal motion at 300 K is added, the effective resolution is estimated to be 0.7 mrad. The coincidence field as well as the flood field used for efficiency correction were collected intermittently to reduce the effects of possible instrumental instabilities. All data were collected in list mode using an 11-μrad channel width. A total of 53×10^6 counts were accumulated. The data displayed C_{2v} symmetry after the efficiency correction, and the statistics was augmented accordingly by symmetrization.[33] In this article the data are presented on a 0.39-mrad mesh.

On the theoretical side, our computations employ the conventional LDA based framework within the Korringa-Kohn-Rostoker (KKR) band-structure scheme in which electrons and positrons are treated as independent particles, see Refs. 34, 15, and 16 for details of our methodology and formalism for evaluating the electron-positron momentum density in a general multiatom per unit cell lattice. Since the electron-positron correlation effects are essentially neglected in this approach, a comparison of the theoretical predictions with the corresponding measurements offers insight into the importance of these effects. The experience with the c-projected data appears to indicate that these effects are relatively small, although this point bears further study.[18]

Concerning computational details, the specific electron and positron muffin-tin potentials employed in this work are identical to those used in our earlier study of the c projection.[15,16] In order to obtain the a projection along the high-symmetry lines in the ΓYTZ plane, the electron energy bands and wave functions were first calculated on a 26×26 **k**-point grid on the bottom (ΓXSY) and top ($ZURT$) planes of the irreducible Brillouin zone, and a 26×11 **k**-point grid on the vertical ΓXUZ and $YSRT$ planes; see Fig. 1. The 3D electron-positron momentum density $\rho_{2\gamma}(\mathbf{p})$ was next computed at 931 **p** points obtained from each of the **k** points by adding reciprocal lattice vectors, yielding $\rho_{2\gamma}(\mathbf{p})$ in various high-symmetry planes containing the a axis. From this basic data set, the 2D a-axis projected distribution was then computed along the high-symmetry lines in the first as well as higher zones in the (p_z,p_y) plane. A number of test calculations using denser **k** meshes and larger reciprocal-lattice vector sets were carried out in order to ensure that the present choice of parameters accurately accounts for the presence of Fermi surface breaks, and properly treats the fairly complicated high-momentum behavior of $\rho_{2\gamma}(\mathbf{p})$.

As emphasized in Refs. 16 and 13, in comparing theoretical and experimental results we must remember that the calculations involve annihilation between the positron and electrons in Bloch states. The assumption of perfect crystalline periodicity underlying this model implies that the contribution resulting from vacancies, oxygen inhomogeneities, and other defects in the specimen is not included in the theory. Accordingly, in Ref. 13 for the c projection, the measured temperature dependence of the spectra itself was used to correct the data for the presence of such a "background." Here we account for this effect by assuming the background to possess an isotropic Gaussian shape, where the width and weight of the Gaussian are found by making a simultaneous least-squares fit between theory and experiment for the ΓY and ΓZ sections. We are not in a position to apply the more satisfactory approach of Ref. 13, since 2D-ACAR's for the a projection were not measured at a series of temperatures.[35]

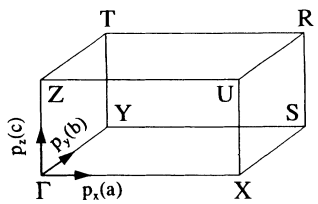

FIG. 1. The irreducible $\frac{1}{8}$ of the first Brillouin zone in Y123 giving notation for various high-symmetry points.

Specifically, we use the relation

$$\tilde{N}(p_y,p_z)=\gamma[N(p_y,p_z)-\beta-\alpha G(p;\sigma)] , \quad (1)$$

where $\tilde{N}(p_y,p_z)$ and $N(p_y,p_z)$ denote the background corrected and the as-measured distribution respectively. $G(p;\sigma)$ is an isotropic Gaussian of standard deviation σ, with $p=\sqrt{p_y^2+p_z^2}$. α gives the weight of the Gaussian background, and γ allows $\tilde{N}(p_y,p_z)$ to be renormalized. The parameter β accounts for small differences between theory and experiment at high momenta where the measured spectrum does not go to zero due to random coincidences, small-angle scattering, etc. Equation (1) was used to obtain the best fit between $\tilde{N}(p_y,p_z)$ and the theoretical distribution along the ΓZ and ΓY directions and yielded a fairly broad Gaussian background of FWHM=10.4 mrad, comparable to the FWHM of about 12 mrad of the measured spectrum. The parameter α allows us to estimate that 34% of all annihilations are associated with the correction; this result is consistent with our earlier estimates of the background intensity for this particular sample, which was studied previously in the c projection.[9,13,35] Figure 2 illustrates the effect of the background correction. The correction reduces the spectral intensity for low momenta as seen from the upper section; in contrast, there is little effect at momenta greater than about 6 mrad. Cuts through higher zones, more than 6 mrad away from the center are less affected as seen from the lower section in Fig. 2.

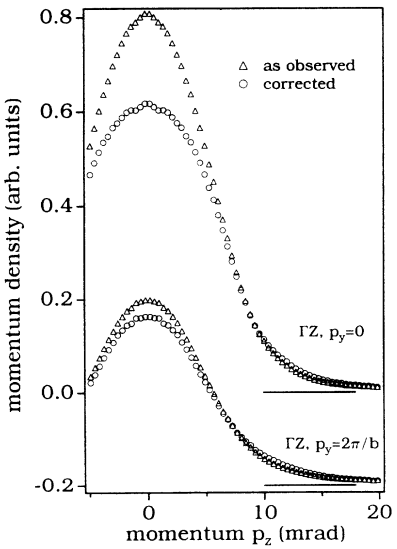

FIG. 2. Two typical sections (offset vertically with respect to each other) through the as observed a-projected 2D-ACAR spectrum of Y123 are compared with the corresponding results obtained after applying the background correction described in the text [see discussion of Eq. (1)]. The upper section refers to the ΓZ line through $p=0$, while the lower section is for an off-center line parallel to ΓZ passing through $p_y=2\pi/b$. The momentum is in milliradian (mrad) units, where 1 mrad=0.137 a.u.

III. RESULTS AND DISCUSSION

Figure 3 shows the as measured 2D-ACAR spectrum which, as expected, resembles a featureless "mountain." In order to expose fine structure in the data, the anisotropic spectrum

$$A(p_y,p_z)=\tilde{N}(p_y,p_z)-S(p) , \quad (2)$$

obtained by subtracting a smooth surface $S(p)$ from the measured distribution is also shown. The specific function $S(p)$ used here is obtained by smoothing the experimental spectrum. Although the resulting $A(\mathbf{p})$ depends on $S(\mathbf{p})$, the structures in $A(\mathbf{p})$, our main concern, are to a large degree insensitive to the specific choice of $S(\mathbf{p})$. Notably, we see the presence of a ridgelike structure running parallel to the p_z direction through $p=0$, as well as the related first and second umklapp images at about ± 6 mrad and ± 12 mrad.

Figure 4 compares a number of sections through the experimental 2D-ACAR distribution after background correction [see Eq. (1)] with the corresponding theoretical predictions. An excellent accord is seen not only for sections close to or intersecting the Γ point at $p=0$ [the uppermost sections in Figs. 4(a) and 4(b)], but also for sections at higher momenta in the (p_y,p_z) plane. A comparison of Figs. 2 and 4 makes it clear that without the background correction, the experimental spectrum is substantially more peaked around $p=0$, as is also the case for the earlier c projected data.[13] The correction essentially removes this discrepancy throughout momentum space and better reveals the anisotropy of the spectrum, as seen for example by comparing the ΓZ and ΓY sections passing through $p=0$ in Fig. 4. The absolute size of the anisotropy in Fig. 4 is of course quite small—a maximum of about 5% of the peak height—so that the overall distribution is still quite isotropic. For example, the ΓY as well as the ΓZ sections decrease to half their peak value (at $p=0$) by about 6.8 mrad, and to 10% of the peak by about 11.0 mrad. Incidentally, a very similar overall shape of the spectrum is presented by the c projected 2D-ACAR data.[13]

Since all occupied electron states contribute to the 2D-ACAR spectrum, the part arising from partially filled bands, related to the fermiology of Y123,[36-39] constitutes only a few percent of the total spectral intensity. In this connection, we define a theoretical anisotropic distribution by subtracting the *same* isotropic surface $S(p)$ used in Eq. (2) above to obtain the experimental anisotropy $A(p_y,p_z)$. We focus first on the ΓY section in which the band theory predicts FS crossings. Figure 5 shows that the theoretical ΓY anisotropy (uppermost curve) is in good overall accord with the measurements with respect to both the absolute amplitude as well as much of the major structure in the data.

Insight into the nature of FS signatures is provided by the lowest curve in Fig. 5, which gives the a-axis integral F_a of the 3D occupation function $F(\mathbf{k})$ defined as the total number of occupied bands at any $\mathbf{k}$ point in the Brillouin zone. Aside from being periodic, $F(\mathbf{k})$ differs from $\rho_{2\gamma}(\mathbf{p})$ in that $F(\mathbf{k})$ neglects the electron-positron matrix element, allowing some understanding of the interplay

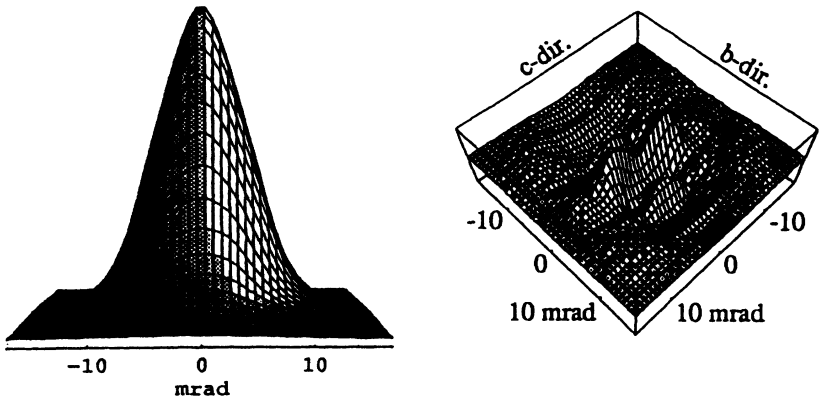

FIG. 3. The as observed a-projected 2D-ACAR spectrum in Y123 (left) and the corresponding anisotropic spectrum (right).

between the effects of matrix elements and FS breaks on the 2D ACAR's. Bearing these considerations in mind, we delineate first the structure in the a projection F_a of $F(\mathbf{k})$, the lowest curve, keeping in mind Fig. 6, which gives the FS cross sections in the ΓXSY plane. Starting from Γ, F_a remains flat as we move along ΓY until the Cu-O chain-related ridge FS empties at r_0. The relative sharpness of the break at r_0 reflects the fact that the band giving rise to the ridge FS is nearly dispersionless along the a axis, while the size of the break at r_0 is related to the size of the ridge FS. We next encounter the two closely spaced breaks B_1 and B_2 associated with the CuO_2 plane derived barrel FS's. These breaks are slightly less sharp than r_0 due to the somewhat greater dispersion of the associated bands. The remaining FS sheets, namely, the pillbox (p) and the butterflies, do not give a substantial signature in F_a due presumably to their small size.

F_a is modified drastically when the electron-positron matrix element is included as seen from the middle curve in Fig. 5, which gives the theoretical ΓY anisotropy before the resolution broadening is folded in. The break r_0 is seen clearly in the middle curve but the breaks B_1 and B_2 have virtually disappeared. This is the result of the tendency of the positron to be localized in the region of the Cu-O chains, so that there is little positron charge in the CuO_2 planes, causing the coupling between the positron and the CuO_2 plane bands to be weak and the related FS breaks to be small.[15,17,20,40] The electron-positron matrix element also alters the relative size of the break from the ridge FS in the first Brillouin zone (BZ) compared to its size at umklapp images in higher BZ's. In particular, the second umklapp image (r_2,r_2') is somewhat stronger than the first image (r_1,r_1'). We see that breaks on the left side (r_1',r_2') are smaller than the corresponding breaks on the right-hand side (r_1,r_2) of the second and third Γ points. These are effects of the detailed nature of the underlying Bloch electron wave functions. Interestingly, the bump M around 2.5 mrad in the middle curve is not a FS signature but a matrix element effect.

Having clarified the origin of structure in the theoretical ΓY section, we are in a position now to identify FS signatures in the experimental spectrum of Fig. 5. The

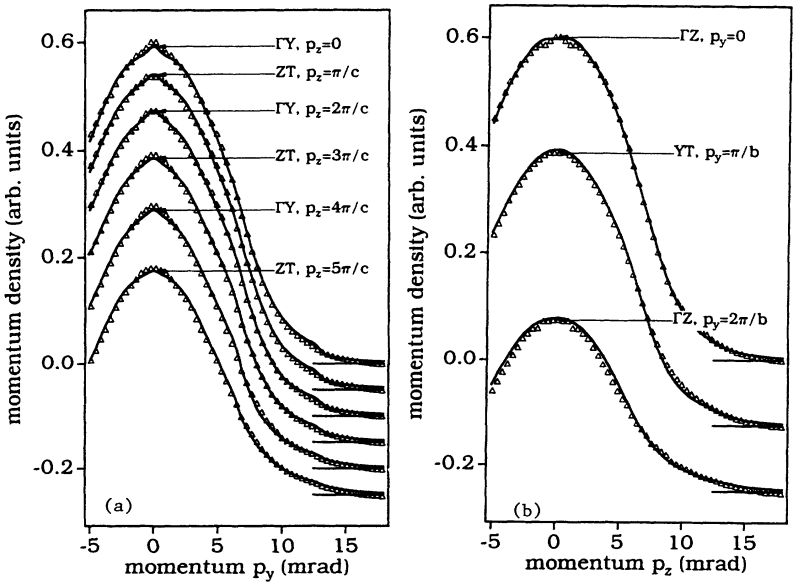

FIG. 4. A comparison of various cuts (offset vertically with respect to each other) through the background corrected 2D-ACAR data (open triangles) with the corresponding theoretical predictions (solid lines) along lines parallel to (a) ΓY for various indicated p_z values and (b) lines parallel to ΓZ for three p_y values. The theoretical curves have been broadened to reflect experimental resolution. The spectra are symmetric around $p=0$ but are shown extended to negative p values to reveal the structure around $p=0$ clearly.

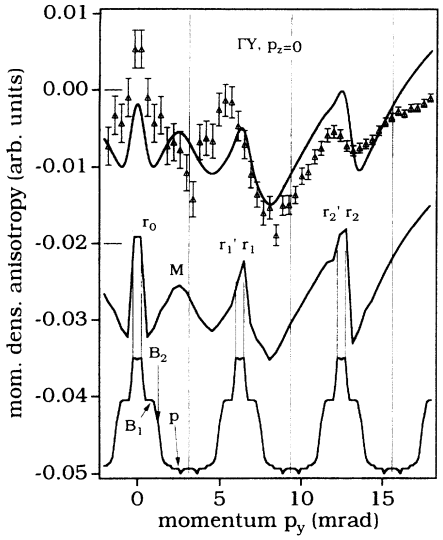

FIG. 5. A comparison of the theoretically predicted momentum density anisotropy (uppermost solid line) with the corresponding experimental result along the ΓY line passing through $p=0$. The middle curve (offset vertically from the upper curve) gives the theoretical result without resolution broadening and shows Fermi surface breaks in the distribution more clearly. The lowest periodic curve gives the a-axis projection (arbitrary scale) of the 3D occupation number density defined as the number of filled bands at any point in $\mathbf{k}$ space and shows the effects of Fermi surface in a simple model, which neglects the electron-positron matrix element. Various letters denote spectral features discussed in the text. Vertical lines mark the zone boundaries along ΓY.

rapid variation in the measured anisotropy near $p=0$ is clear evidence of the ridge FS; the fact that the sharpness of the two upper curves is similar around $p=0$ further indicates that the data is consistent with a fairly small ridge dispersion along the a-axis implicit in the calculations. There is also a reasonable accord in the region of the first ridge image around 6.3 mrad, the breaks r_1 and r_1'. The impression of the second ridge image around 12.3 mrad, r_2 and r_2', is somewhat weaker in the data compared to theoretical prediction. On the whole the measured ΓY section contains strong evidence of the ridge FS. The level of discrepancies seen in Fig. 5, including the region of the non-FS related bump M, is comparable to those encountered previously in connection with the c projection.[13] The origin of these discrepancies is unclear, but they can arise from various mechanisms including inaccuracies in the theoretical description of the positron and electron wave functions and the approximations in the theory in treating electron-positron and electron-electron correlations.

A deeper understanding of the signature of the ridge FS is offered by Fig. 7, which considers characteristic variations in spectral shape for a series of spectra parallel to the p_y direction for different p_z values. Systematic changes in the theoretical spectra are evident as we move from the $p_z=0$ (uppermost) ΓY section to the $p_z=5\pi/c$ (lowest) section and consist of (i) an increase in the size of the feature r_0 with increasing p_z with a maximum around $p_z=3\pi/c$, the feature subsequently reduces in size, (ii) a reduction in the size of the matrix element related bump M up to $p_z=4\pi/c$, followed by a relative increase in its size in the $p_z=5\pi/c$ curve, (iii) an increase in the size of the first umklapp peak (r_1',r_1) up to about $p_z=4\pi/c$, followed by a relative decrease in the $p_z=5\pi/c$ curve, and (iv) a continuous decrease in the size of the second ridge umklapp feature (r_2',r_2). The preceding theoretical predictions are more or less consistent with the experimental data of Fig. 7, especially when we keep the statistics in mind. In particular, in going from $p_z=0$ to $5\pi/c$, the second image of the ridge around 12.6 mrad in the experimental data decreases continuously in size; the matrix element related feature M around 2.5 mrad, visible in the form of a weak shoulder, decreases in size up to $p_z=4\pi/c$ with a hint of its reemergence at $p_z=5\pi/c$. The $p=0$

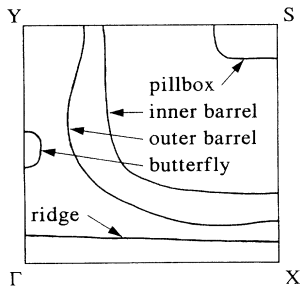

FIG. 6. Cross sections of various Fermi surface sheets in the ΓXSY plane of the Brillouin zone in Y123.

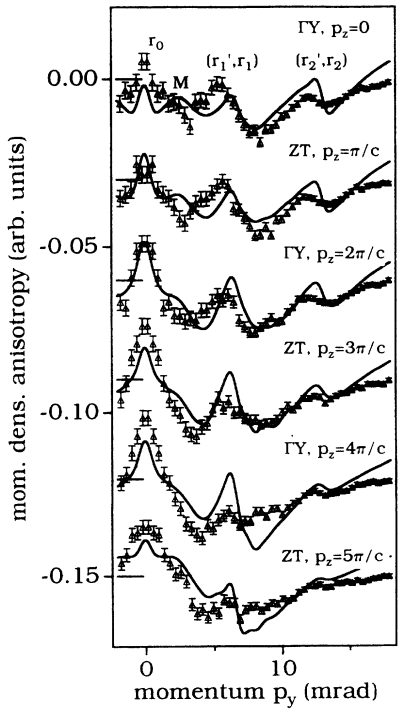

FIG. 7. A comparison of changes in shapes of theoretical (solid) and experimental anisotropic spectra for a series of sections parallel to the p_y direction for various indicated p_z values. Various letters denote features discussed in the text.

peak in the data appears to become more prominent up to $p_z = 4\pi/c$ followed by a relative decrease in its size in the $p_z = 5\pi/c$ section. Finally, although the 6.3-mrad first ridge image is visible in all the experimental sections shown in Fig. 7, its detailed behavior appears to differ from theory in that its amplitude decreases continuously in size with increasing p_z in the data rather than undergo an increase up to $p_z = 4\pi/c$ followed by a decrease.

Figure 8 considers several cuts parallel to the p_z direction for different values of p_y. There are no FS crossings along the ΓZ line passing through $p = 0$ and all the structure in the theoretical spectra of Fig. 8 essentially results from matrix element effects. There is a reasonable accord between the theory and data in the ΓZ $p_y = 0$ section (uppermost), although the bump in the measurements around 11 mrad is missing in the calculations. The middle section in Fig. 8 shows discrepancies for momenta greater than about 5 mrad, while the lowest section shows little accord, although we should keep in mind that the overall amplitude of anisotropy here is relatively small. These discrepancies arise presumably from mechanisms similar to those noted in connection with Fig. 5 above.

Our discussion so far has involved the background corrected experimental 2D-ACAR data and its comparison with the corresponding theoretical predictions. Some insight into the extent to which our conclusions concerning the presence of FS related fine structure in the data are insensitive to the treatment of background is provided by Fig. 9, which considers the ΓY-ΓZ difference where both sections pass through $p = 0$. The advantage of using such difference sections is that the underlying isotropic part of the distribution, including much of the background contribution, which is expected to be essentially isotropic, automatically gets subtracted, allowing one to focus on the structure in the data without requiring an explicit knowledge of the shape or the weight of the background function. Despite the success of such an approach in analyzing c-projected 2D-ACAR spectra,[13] the interpretation of a difference section is intrinsically complicated by the fact that information from two independent directions is involved in the presence of effects

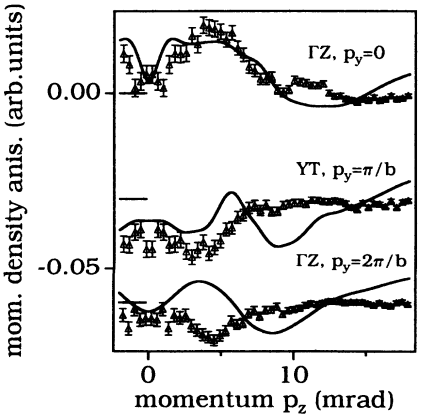

FIG. 8. Same as the caption to Fig. 7 except that sections parallel to the p_z direction are considered for various p_y values.

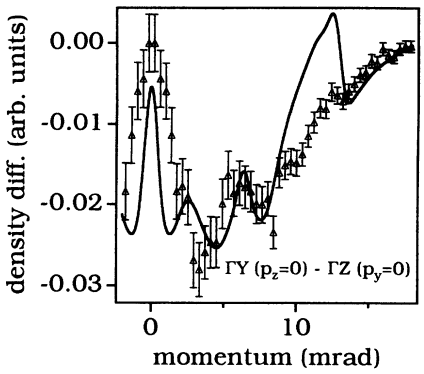

FIG. 9. The theoretical (solid) and experimental difference spectrum ΓY-ΓZ is compared where both sections pass through $p = 0$. The experimental data here is *without* background correction.

of finite experimental statistics and resolution. In any event, Fig. 9 shows a reasonable accord between the computed and measured shape of the ΓY-ΓZ difference. Interestingly, the theoretical $p = 0$ ridge feature is in better accord with the data in Fig. 9 compared to the representation of Fig. 5.

IV. CONCLUSIONS

We have presented theoretical and experimental results for the a-axis-projected positron 2D-ACAR spectrum from $YBa_2Cu_3O_{7-x}$. Extensive comparisons show that there is reasonable agreement between theory and experiment as to the overall shape as well as the fine structure in the spectra. As in the previous work on the c-projected 2D-ACAR data,[13] we found it necessary to correct the as observed spectrum for an isotropic background due presumably to vacancies, oxygen inhomogeneities, and other defects, whose contribution is not included in the computations. We establish clearly the presence in the data of the theoretically predicted signature of the electron ridge FS related to the Cu-O chains around $p = 0$; the first and second umklapp images of the ridge FS at about 6.3 and 12.6 mrad are also identified. The discrepancies between theory and experiment with regard to the details of the momentum dependence of the electron-positron matrix element are probably inherent in first-principles comparisons of the present sort, and are not considered serious. The a-axis results of this study, when combined with the previous work on the c projection, make a strong case that the conventional LDA-based band-theory framework provides a good description of the electron momentum distribution in the metallic Y123 compound, at least as seen via the positron spectroscopy.

This study has implications, albeit indirect, concerning the question of possible localization of electron states along the c direction.[31,1-4] Our theoretical approach fundamentally assumes delocalized Bloch wave functions to represent the annihilating positron and electrons. If the electrons were localized along the c axis we would presumably find a substantial deviation between band-

theory predictions and the measured spectra along the c direction compared to the in-plane directions. No such effect is, however, seen in the present extensive comparisons—the band theory appears to describe the a-axis- and the c-axis-projected 2D ACAR's more or less equally well. The width and shape of the a-projected 2D ACAR along the c direction are very similar to those in the in-plane b direction, and also to those of the c-projected 2D ACAR in the a-b plane (localization along the c axis may be expected to spread out the momentum distribution). FS signatures, including higher-momentum images, are seen equally well in the a- and c-projected 2D-ACAR's. Taken together, these observations do not support the localization of electronic states, at least not strongly, along the c axis in Y123. We should keep in mind, however, that conclusions based on the positron spectroscopy in Y123 would tend to be weighted towards the behavior of the Cu-O chain related group of electrons due to the preferential sampling of these electrons by the positron.

ACKNOWLEDGMENTS

This work is supported by the U.S. Department of Energy under Contract No. W-31-109-ENG-38, including a subcontract to Northeastern University, and has benefited from travel grants from the NSF and NATO, and the allocation of supercomputer time at NERSC and the Pittsburgh Supercomputer Centers. It was also sponsored by the National Computer Facilities Foundation (NCF) with financial support from the Netherlands Organization for Scientific Research (NWO).

---

*Permanent address: Physics Department, Tampere University of Technology, Tampere, Finland.

[1]For recent discussions concerning the electronic structures, fermiology, and spectroscopy of high T_c's see Refs. 2–4.

[2]*Fermiology of High-T_c Superconductors,* edited by A. Bansil, A. J. Arko, R. Benedek, V. J. Emery, and L. C. Smedskjaer [J. Phys. Chem. Solids **52**, No. 11/12 (1991)].

[3]*Electronic Structure and Fermiology of High-T_c Superconductors,* edited by T. Takahashi, A. Bansil, and H. Katayama-Yoshida [J. Phys. Chem. Solids **53**, No. 12 (1992)].

[4]*Spectroscopies in Novel Superconductors,* edited by F. M. Mueller, A. Bansil, and A. J. Arko [J. Phys. Chem. Solids **54**, No. 10 (1993)].

[5]For early work on twinned Y123 crystals, see Refs. 6–8; for the more recent studies of untwinned single crystals see Refs. 9–14.

[6]M. Peter, L. Hoffmann, and A. A. Manuel, Physica C **153-155**, 1724 (1988); L. Hoffmann, A. A. Manuel, M. Peter, E. Walker, and M. A. Damento, Europhys. Lett. **6**, 61 (1988); Physica C **153-155**, 129 (1988); M. Peter and A. A. Manuel, Phys. Scr. T **29**, 106 (1989).

[7]L. C. Smedskjaer, J. Z. Liu, R. Benedek, D. G. Legnini, D. J. Lam, M. D. Stahulak, H. Claus, and A. Bansil, Physica C **156**, 269 (1988).

[8]H. Haghighi, J. H. Kaiser, S. Rayner, R. N. West, M. J. Fluss, R. H. Howell, P. E. A. Turchi, A. L. Wachs, Y. C. Jean, and Z. Z. Wang, J. Phys. Condens. Matter **2**, 1911 (1990).

[9]L. C. Smedskjaer, A. Bansil, U. Welp, Y. Fang, and K. G. Bailey, J. Phys. Chem. Solids **52**, 1541 (1991).

[10]L. Hoffmann, W. Sadowski, A. Shukla, Gh. Adam, B. Barbiellini, and M. Peter, J. Phys. Chem. Solids **52**, 1551 (1991); A. A. Manuel, B. Barbiellini, M. Gauthier, L. Hoffmann, T. Jarlborg, S. Massidda, M. Peter, W. Sadowski, A. Shukla, and E. Walker, J. Phys. Chem. Solids **54**, 1223 (1993).

[11]L. Hoffmann, W. Sadowski, and M. Peter, Mater. Sci. Forum **105-110**, 647 (1992).

[12]H. Haghighi, J. H. Kaiser, S. Rayner, R. N. West, J. Z. Liu, R. Shelton, R. H. Howell, F. Solar, and M. J. Fluss, J. Phys. Chem. Solids **52**, 1535 (1991); Phys. Rev. Lett. **67**, 382 (1991).

[13]L. C. Smedskjaer, A. Bansil, U. Welp, Y. Fang, and K. G. Bailey, Physica C **192**, 259 (1992); L. C. Smedskjaer and A. Bansil, Mater. Sci. Forum **105-110**, 459 (1992).

[14]L. C. Smedskjaer, A. Bansil, U. Welp, Y. Fang, and K. G. Bailey, Phys. Rev. B **46**, 5868 (1992).

[15]A. Bansil, R. Pankaluoto, R. S. Rao, P. E. Mijnarends, R. Prasad, and L. C. Smedskjaer, Phys. Rev. Lett. **61**, 2480 (1988); A. Bansil, J. Phys. Chem. Solids **52**, 1493 (1991); A. Bansil, P. E. Mijnarends, and L. C. Smedskjaer, Phys. Rev. B **43**, 3667 (1991).

[16]A. Bansil, P. E. Mijnarends, and L. C. Smedskjaer, Physica C **172**, 175 (1990).

[17]S. Massida, Physica C **169**, 137 (1990); S. Massida, J. Yu, A. J. Freeman, L. Hoffmann, P. Genoud, and A. A. Manuel, J. Phys. Chem. Solids **52**, 1503 (1991).

[18]T. Jarlborg, B. Barbiellini, E. Boronski, P. Genoud, and M. Peter, J. Phys. Chem. Solids **52**, 1515 (1991).

[19]B. Barbiellini, P. Genoud, J. Y. Henry, L. Hoffmann, T. Jarlborg, A. A. Manuel, S. Massida, M. Peter, W. Sadowski, H. J. Scheel, A. Shukla, A. K. Singh, and E. Walker, Phys. Rev. B **43**, 7810 (1991).

[20]S. Berko, D. J. Singh, and E. C. von Stetten, J. Phys. Chem. Solids **52**, 1485 (1991); D. Singh, W. E. Pickett, E. C. von Stetten, and S. Berko, Phys. Rev. B **42**, 2696 (1990).

[21]See, e.g., A. Bansil, Zeits. für Natur. **48A**, 165 (1993).

[22]J. C. Campuzano, G. Jennings, A. J. Arko, R. S. List, B. W. Veal, and R. Benedek, J. Phys. Chem. Solids **52**, 1411 (1991); J. C. Campuzano, L. C. Smedskjaer, R. Benedek, G. Jennings, and A. Bansil, Phys. Rev. B **43**, 2788 (1991); J. C. Compuzano, G. Jennings, M. Faiz, L. Beaulaigue, B. W. Veal, J. Z. Liu, A. P. Paulikas, K. Vanderwoort, H. Claus, R. S. List, A. J. Arko, and R. J. Bartlett, Phys. Rev. Lett. **64**, 2308 (1990).

[23]C. G. Olson, J. G. Tobin, F. R. Solal, C. Gu, J. Z. Liu, M. J. Fluss, R. H. Howell, J. C. O'Brien, H. B. Radousky, and P. A. Sterne, J. Phys. Chem. Solids **52**, 1419 (1991); J. G. Tobin, C. G. Olson, C. Gu, J. Z. Liu, F. R. Solal, M. J. Fluss, R. H. Howell, J. C. O'Brien, H. B. Radousky, and P. A. Sterne, Phys. Rev. B **45**, 5563 (1992).

[24]C. M. Fowler, B. L. Freeman, W. L. Hults, J. C. King, F. M. Mueller, and J. L. Smith, Phys. Rev. Lett. **68**, 534 (1992); F. M. Mueller, J. Phys. Chem. Solids **52**, 1457 (1991).

[25]G. Kido, K. Komorita, H. Katayama-Yoshida, and T. Takahashi, J. Phys. Chem. Solids **52**, 1465 (1991).

[26]P. E. Mijnarends, A. F. J. Melis, and A. W. Weeber, J. Phys. Chem. Solids **52**, 1569 (1991); P. E. Mijnarends, A. F. J. Melis, A. W. Weeber, A. A. Menowsky, and K. Kadowaki, Physica C **176**, 113 (1990).

[27]L. P. Chan, D. R. Harshman, K. G. Lynn, S. Massida, and D. B. Mitzi, J. Phys. Chem. Solids **52**, 1557 (1991); Phys. Rev. Lett. **67**, 1350 (1991).

[28]R. N. West, J. Phys. Chem. Solids **53**, 1669 (1992).

[29]P. A. Sterne, R. H. Howell, M. J. Fluss, J. H. Kaiser, K. Kitazawa, and H. Kojima, J. Phys. Chem. Solids **54**, 1231 (1993).

[30]P. Blandin, S. Massidda, B. Barbiellini, T. Jarlborg, P. Lerch, A. A. Manuel, L. Hoffmann, M. Gauthier, W. Sadowski, E. Walker, M. Peter, Jaejun Yu, and A. J. Freeman, Phys. Rev. B **46**, 390 (1992).

[31]P. W. Anderson (unpublished).

[32]L. C. Smedskjaer, R. Pankaluoto, A. Bansil, and P. E. Mijnarends, J. Phys. Chem. Solids **54**, 1239 (1993).

[33]L. C. Smedskjaer and D. G. Legnini, Nucl. Instrum. Methods Phys. A **292**, 487 (1990).

[34]P. E. Mijnarends and A. Bansil, J. Phys.: Condens. Matter **2**, 911 (1990).

[35]We have, however, used the present approach to handle the background correction for the *c*-projected spectra of Ref. 13 and found the results to be essentially the same as those obtained by using the temperature dependence of the spectra. Our specific estimate of the weight of the background (about 34%) is in line with the intensity of the second lifetime component reported in some positron lifetime studies, see for example, Ishibashi *et al.*, J. Phys.: Condens. Matter **3**, 9169 (1991).

[36]See Refs. 37–39 for band-structure calculations of Y123.

[37]J. Yu, S. Massidda, A. J. Freeman, and D. D. Koelling, Phys. Lett. A **122**, 203 (1987).

[38]W. E. Pickett, R. E. Cohen, and H. Krakauer, Phys. Rev. B **42**, 8764 (1990).

[39]C. O. Rodriguez, A. I. Liechtenstein, I. I. Mazin, O. Jepsen, O. K. Andersen, and M. Methfessel, Phys. Rev. B **42**, 2692 (1990).

[40]A rather weak imprint of the barrel Fermi surfaces is seen to remain in Fig. 5 (middle curve), especially at higher momenta. However, this signature would be difficult to resolve in a positron experiment.

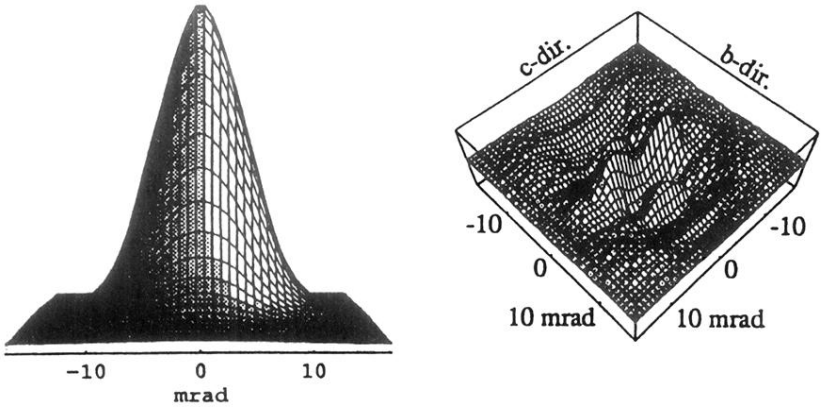

FIG. 3. The as observed *a*-projected 2D-ACAR spectrum in Y123 (left) and the corresponding anisotropic spectrum (right).